Morphologic Phenotyping with MR Microscopy: The Visible Mouse[1]

G. Allan Johnson, PhD
Gary P. Cofer, MS
Sally L. Gewalt, MS
Laurence W. Hedlund, PhD

Index terms:
Animals
Magnetic resonance (MR), technology
Special Reports

Published online before print
10.1148/radiol.2223010531
Radiology 2002; 222:789–793

Abbreviations:
TE = echo time
TR = repetition time
3D = three-dimensional

[1] From the Center for In Vivo Microscopy, Duke University Medical Center, Rm 141, D Bryan Neuroscience Bldg, Research Dr, Durham, NC 27710. Received March 5, 2001; revision requested April 14; final revision received September 5; accepted September 6. Supported by the National Institutes of Health National Center for Research Resources (P41 RR05959). **Address correspondence to** G.A.J. (e-mail: *gaj@orion.mc.duke.edu*).

G.A.J. is a cofounder of MRPath, formed to commercialize the application of magnetic resonance histology. L.W.H. and S.L.G. have consulted for the company.

Author contributions:
Guarantor of integrity of entire study, G.A.J.; study concepts and design, G.A.J., L.W.H., S.L.G., G.P.C.; literature research, G.A.J.; experimental studies, G.A.J.; data acquisition, G.A.J., L.W.H., G.P.C.; data analysis/interpretation, G.A.J., L.W.H.; manuscript preparation, G.A.J., L.W.H., S.L.G., G.P.C.; manuscript definition of intellectual content, G.A.J.; manuscript editing, G.A.J., L.W.H., S.L.G.; manuscript revision/review and final version approval, G.A.J., L.W.H., S.L.G., G.P.C.

A method for rapid morphologic phenotyping is demonstrated by using magnetic resonance microscopy. Whole fixed C57BL/6J mice were imaged at 110-μm isotropic resolution; limited volumes of the intact specimen, at 50-μm isotropic resolution; and isolated organs, at 25-μm isotropic resolution. The three-dimensional imaging technique was applied to uricase knockout mice to demonstrate the method for the evaluation of morphologic phenotype.

Supplemental material: (*radiology.rsnajnls.org/cgi/content/full/2223010531/DC1*)

Rapid developments in molecular biology have created extraordinary opportunities to understand the connection between specific genotype, structure, and function. This, in turn, has created demand for effective methods of phenotyping. In 1999, more than 2 million transgenic and knockout mice were bred for research, with an estimate of more than 6 million animals in the past year (1). Magnetic resonance (MR) imaging has been used to characterize neuroanatomy in clinical studies with well-documented human genotypes (2–4). MR imaging and microscopy have also been applied to phenotype a number of animal models (5,6). The purpose of our report is to present a method for morphologic phenotyping by using MR microscopy to allow scientists to nondestructively image the whole mouse ("The Visible Mouse") with isotropic three-dimensional (3D) spatial resolution as small as 110 μm (1×10^{-3} mm^3) and spatial resolution in isolated organs as small as 25 μm (1.6×10^{-5} mm^3).

IMAGE ACQUISITION WITH VERY LARGE ARRAYS

All studies were performed in accordance with our institutional animal care and use committee. Male C57BL/6J mice ($n = 24$) were obtained from commercial sources (Jackson Laboratory, Bar Harbor, Me). Uricase knockout mice ($n = 4$) used to demonstrate a specific phenotype were supplied from a colony maintained at the Duke University Medical Center (7).

The founders of MR imaging clearly envisioned the potential for MR microscopy, but the adaptation to practice has required considerable technical development (8,9). For microscopic imaging, MR imaging has been improved by means of performance at higher magnetic field strengths, use of improved encoding strategies, and use of specialized radio-frequency coils (10–12). Prior to this study, the highest spatial resolution was obtained in limited fields of view that were not practical for whole-mouse examination. In previous efforts, we overcame two limitations—limited sensitivity and limited field of view (coverage)—that now allow us to examine the whole mouse at microscopic resolution. These barriers have been addressed with the development of 3D encoding with very large image arrays and the use of active stains. Images were acquired with three modified MR imagers (Signa; GE Medical Systems, Milwaukee, Wis). The critical characteristics of each system are summarized in Table 1. All three systems used shielded gradients and were controlled by consoles (Signa 5X; GE Medical Systems) that have been modified for MR microscopy. The 3D spin-echo images (50/5, repetition time [TR] msec/echo time [TE] msec) were acquired, as defined in Table 2. The number of signals acquired was chosen so that the total acquisition time for each study was 14.5 hours (ie, less than a single overnight session).

The 3D encoding was proposed early in the development of MR imaging (13,14). As the technology matured, larger isotropic image arrays became possible (15). We have extended the technology even further by separating the acquisition, reconstruction, archiving, and distribution systems and by optimizing each for the large data sets. Raw data acquired with the imaging systems are transferred to a dedicated 64-bit reconstruction engine (Silicon Graphics, Mountain View, Calif) that can accommodate image arrays as large as $2{,}048^3$. An efficient 3D Fourier transform routine has been implemented with sufficient memory (1 Gbyte), local disk space (200 Gbyte), archive capacity (CD-ROM), and network bandwidth (100 Mbyte/sec) to routinely accommodate large data sets. For example, the raw data for the 512^3-image array is 1 Gbyte. Reconstruction time is approximately 1 hour. Images are analyzed locally with software (VOXELVIEW; Vital Images, Minneapolis, Minn) performed on a workstation (SGI O2, Mountain View, Calif) with 1 Gbyte of memory. The critical array dimensions for all images are included in Table 2.

TABLE 1
Critical Performance Characteristics of the MR Microscopes

Parameters	Field Strength (T)		
	2.0	7.1	9.4
Gradient (mT/m)	180	650	860
Maximum imaging volume (mm)	150 × 150 × 150	40 × 40 × 40	30 × 30 × 30
Radio-frequency coil	Solenoid	Birdcage	Solenoid

TABLE 2
Acquisition Parameters

Region	Field Strength (T)	Array	Signals Acquired	Resolution (μm)	Voxel (μm^3)
Whole mouse	2.0	256 × 256 × 1,024	16	110 × 110 × 110	1.3
Abdomen	7.1	512 × 512 × 512	4	50 × 50 × 50	0.125
Kidney	9.4	256 × 512 × 512	8	25 × 25 × 25	0.016

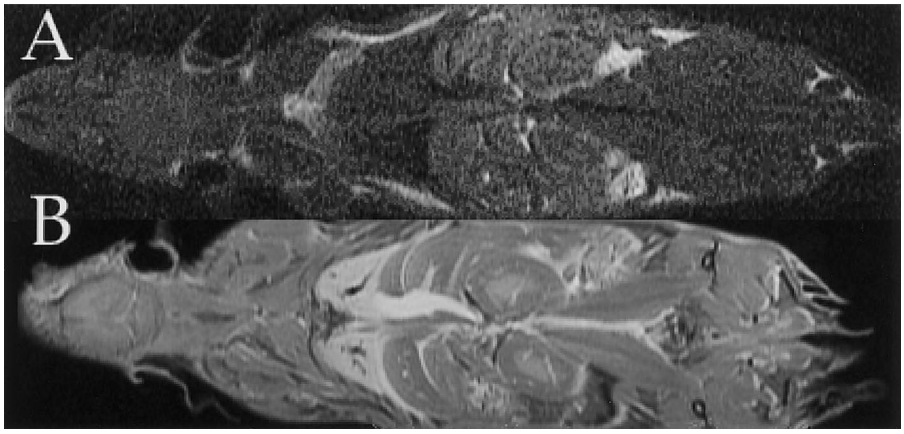

Figure 1. Coronal 2-mm-thick sections were acquired in *(A)* a formalin-fixed specimen and *(B)* a specimen stained with a 1:20 mixture of gadopentetate dimeglumine and formalin. At TR of 100 msec, the gain in signal-to-noise ratio is fivefold greater than that for all tissues except fat.

SPECIMEN PREPARATION: THE ACTIVE STAIN

The second critical element required to create the "Visible Mouse" is the development of active-staining techniques. The use of contrast agents in MR imaging is not new. Paramagnetic molecules used as agents to modify tissue relaxation were first suggested by Mendonca-Dias et al (16). Substantial research has focused on the development of these agents for human use (17). We use the term *active staining* to refer to the use of contrast agent in conjunction with perfusion fixation to provide some specific benefit for MR histologic examination. In this application, we are using active stains to reduce the effective T1 of all the tissues and thus increase the signal-to-noise ratio. With careful control of the vascular access routes, one can produce intact specimens with uniform reduction in spin-lattice relaxation time in the majority of tissue. Systemic perfusion of C57BL/6J mice and uricase knockout mice was performed (L.W.H.) via the right jugular vein and the left carotid artery with 10% buffered formalin (Fisher Scientific, Fairlawn, NJ) and gadopentetate dimeglumine (Magnevist; Berlex Laboratories, Wayne, NJ), a conventional clinical contrast agent at volume ratios ranging from 40:1 to 5:1. The concentration of gadopentetate dimeglumine in 10% buffered formalin has been titrated so that its dilution with water in the fixed tissues results in a T1 of less than 250 msec throughout the tissues.

The efficacy of active stains, the uniformity of the perfusion fixation, and the effect of the agent on the signal-to-noise ratio were measured (G.A.J.) by acquiring a series of seven registered two-dimensional Fourier transform images (2-mm-thick sections, 256 × 512 array over 55 × 110-mm field of view, TE of 5 msec) with TR ranging logarithmically from 20 to 1,280 msec. The resultant data were fit on a pixel-by-pixel basis to the equation $S(x,y,TR) = PD(x,y)(1 - e^{-TR/T1(x,y)})$, where $S(x,y,TR)$ is the signal intensity at position x, y for a given TR, $PD(x,y)$ is the calculated proton-density image, and $T1(x,y)$ is the calculated T1 image.

Morphologic phenotyping with MR microscopy provides the following four attributes that differentiate it from more traditional optical histologic examination: *(a)* MR microscopy is nondestructive, *(b)* contrast in MR microscopy provides unique information about the water in the tissue, *(c)* MR microscopy is inherently 3D, and *(d)* MR microscopy is inherently digital. The results demonstrate a specific comparison between wild type and specific knockout mice in which the morphologic differences are clear. The figures demonstrate these four attributes.

VISIBLE MOUSE

Figure 1 shows a comparison between a formalin-fixed specimen and an identical specimen stained with a 20:1 mixture of formalin and gadopentetate dimeglu-

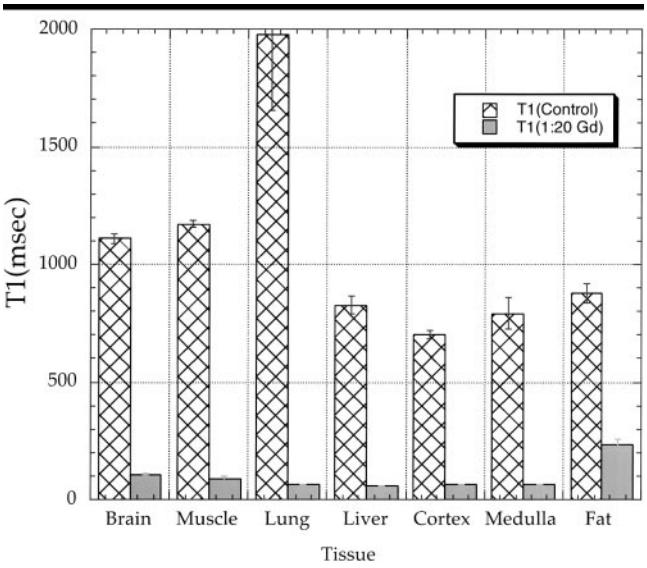

Figure 2. Graph shows the T1 calculated for seven representative tissues in stained *(1:20 Gd)* and unstained *(control)* specimens. The T1 was reduced by more than sixfold in all tissues except fat. *Gd* = gadopentetate dimeglumine.

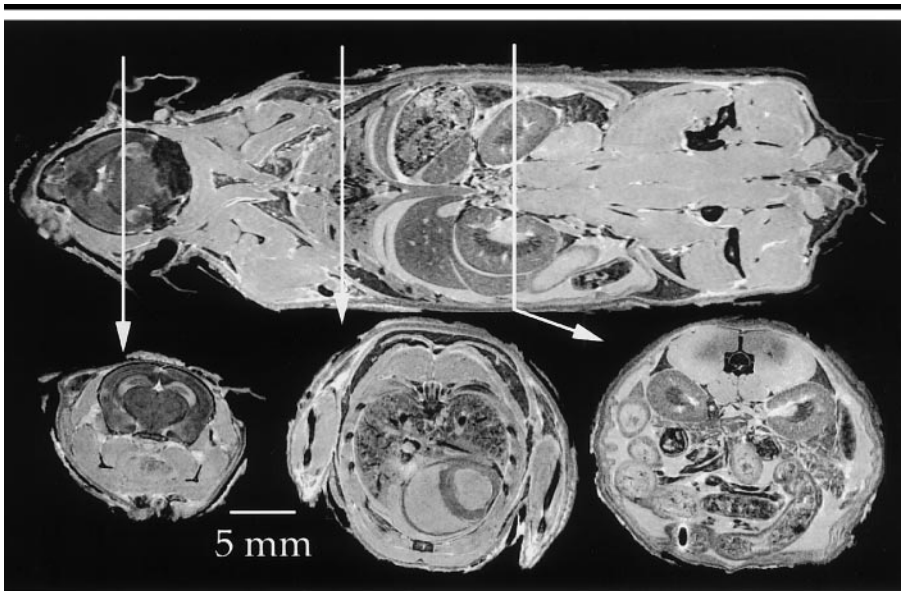

Figure 3. Three-dimensional MR microscopic images with an isotropic array (256 × 256 × 1,024) were acquired in a whole fixed C57BL/6J mouse. The spatial resolution in every plane is 110 × 110 × 110 μm, which allows one to view any arbitrary plane with equal spatial resolution. Coronal (top) and transverse (bottom) images depict 110-μm-thick sections of the head (left), thorax (center), and abdomen (right).

mine. The effect of the stain on signal intensity is clear, with an improvement in signal-to-noise ratio that was sixfold greater in the stained specimen. Even with these relatively thick (2-mm) sections, there is insufficient signal intensity at TR of 100 msec to support any accurate morphometric measurements on images.

A more quantitative assessment of the effect of the stain on various tissues is shown in Figure 2. The T1 was reduced more than sixfold in all tissues except fat. All tissues, except fat, have T1 of less than 150 msec in the stained specimens. The reduction in T1 is less dramatic in fat, which suggests lower penetration of the stain to the fat owing to either the solubility of the stain in fat or differences in vascularity. The T1s of the stained tissues (except fat) tend to converge toward 100 msec so that the ratio of signal improvement is more dependent on T1 in the unstained specimen. Thus, the improvement in signal-to-noise ratio is variable. But a conservative estimate, in which the outer medulla of the kidney was used, showed a signal intensity enhancement that is 5.7-fold greater at TR of 50 msec.

Figure 3 demonstrates the nondestructive nature of MR microscopy. The figure shows a collage derived from the isotropic 110-μm array that covered the whole mouse. Three transverse images obtained with a 1,024 array depict the head, the heart, and the abdomen. Since the sectioning is nondestructive, one can view the data along any arbitrary axis without the distortion that comes from physical sectioning. Because the image array is isotropic, coronal, transverse, and sagittal images can be created from the original (256 × 256 × 1,024) 3D array with the same spatial resolution. The images are three of 1,024 transverse sections and one of 256 coronal sections that depict the mouse from head to tail. Interactive viewers for the 3D image volumes of the whole mouse and the midabdomen discussed in this article (Figs 4, 5) are available as supplemental material (*radiology.rsnajnls.org/cgi/content/full/2223010531/DC1*) on the *Radiology* Web site.

The nondestructive nature of MR microscopy is further evident when Figures 3 and 4 are compared. Because the specimen remains intact, it is possible to reimage the specimen for a limited volume at higher spatial resolution. Figure 4 shows a selected 50-μm coronal section through the kidney from the same wild type animal as shown in Figure 3. This image was acquired at 7.1 T with a 512^3 array with spatial resolution more than 10-fold higher than that shown in Figure 3. Because the specimen remains intact, images from different acquisitions can be aligned since there is no distortion from the physical sectioning that accompanies conventional optical histologic examination. With interactive viewing, it is possible to match the plane from two different image sets very accurately.

Because the tissue has not been dehydrated, as is the case with most conventional optical-staining techniques, the contrast enhancement on all MR images demonstrates unique information about the water and how it is bound in the tissues. This has been one of the major strengths of clinical MR imaging. Contrast enhancement on MR images is the source of extensive study in the MR literature (18,19). We have chosen one of the simplest imaging strategies, that is, a de-

pendence on proton-density and spin-lattice relaxation time (T1).

Quantitative measure of T1 (Fig 2) demonstrated that active staining reduced the T1 of all tissues from a range of 800–2,000 msec (at 2.0 T) to approximately 100 msec. As with conventional MR imaging and microscopy, contrast enhancement is dependent on both the intrinsic tissue parameters (eg, proton density, T1, and T2) and the acquisition strategy (18,19). The parameters in this case include the microstructure of the tissue and the specific methods of active staining. The blood vessels that contain formalin and gadopentetate dimeglumine, which have a high proton density and the shortest T1, are easily identified on all images. At this point, MR contrast enhancement is empirical. The relationship to specific biologic structure is not clear. The understanding and exploitation of the many ways to manipulate contrast enhancement for morphologic phenotyping should be the topic of research in the future. Even without knowledge of the underlying physical principles at work, the current method provides sufficient anatomic contrast enhancement to allow visualization of the internal structures of most of the organs.

The potential of MR microscopy for 3D morphologic phenotyping is demonstrated in Figure 5. The right kidney was excised from an animal, prepared, imaged (as in Fig 3), and imaged again at 9.4 T with a smaller field of view. The 256 × 512 × 256 volume is made up of 25-μm isotropic voxels that are 85-fold smaller than those in Figure 3. Figure 5, *A* shows a 25-μm coronal cross section of vessels and collecting structures. The cortex (outer and inner) and the medulla of the kidney are differentiated. Sampling of the whole organ with isotropic voxels produces data that are ideal for exploration with volume-rendering software. In Figure 5, *B*, we made the tissues with lower signal intensity relatively transparent, yielding a virtual 250-μm section that clarifies the topology of structures as they traverse the thicker section. The 2,500-μm–derived slab in Figure 5, *C* encompasses the entire ventral half of the right kidney, including the major vessels branching through the kidney. The more opaque vessels can be seen in perspective throughout the larger transparent volume. Because there is no distortion from physical sectioning and dehydration that accompany optical methods, these 3D images provide very accurate assessments of organ dimensions, surface areas, and volumes.

The fourth and final attribute of MR microscopy is that the inherent digital nature of the technique allows the data to be shared over the Internet (*radiology.rsnajnls.org/cgi/content/full/2223010531/DC1*). Such atlases will be accessible all over the world for comparative morphologic phenotyping. Figure 5, *B* shows a single coronal level from a uricase knockout mouse acquired in the same fashion as that in Figure 5, *A*. The level in Figure 5, *B* has been interactively selected from the digital atlas to match the level in the wild type mouse in Figure 5, *A*. Common anatomic references (eg, liver and stomach) are seen on both Figure 5, *A* and *B*. The morphologic phenotype in Figure 5, *B* includes an enlarged renal sinus in the kidneys and multiple cortical and medullary cysts. The attributes (eg, multiple planes and volume characterization) noted in Figures 4 and 5 allow more quantitative phenotyping than would be possible with conventional histologic sections. As morphologic measurements (kidney volume, volume of renal sinus, number and location of cysts) are made, they will be stored in the database for comparison with other specimens.

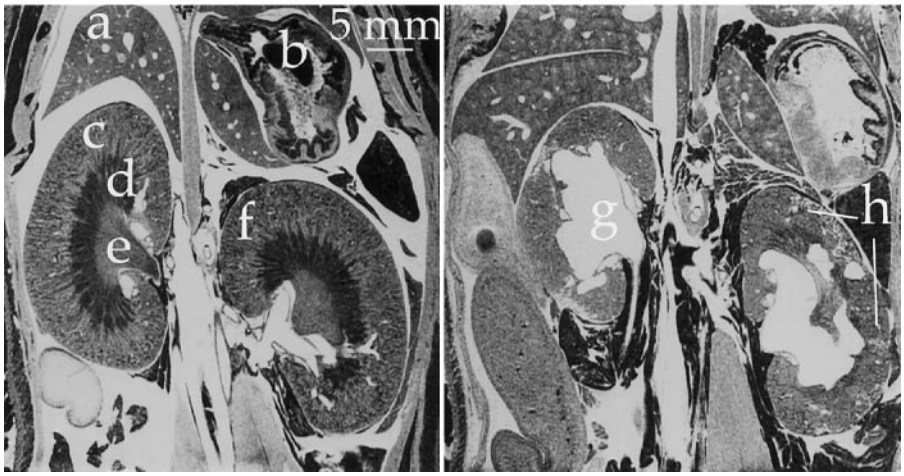

Figure 4. Coronal 3D (512 × 512 × 512) images of control (left) and uricase knockout (right) mice permit morphologic phenotyping. Isotropic resolution of 50 μm allows identification of liver *(a)*, stomach *(b)*, right kidney cortex *(c)*, outer medulla *(d)*, inner medulla-papilla *(e)*, and left kidney cortex *(f)*. In the uricase knockout mouse (right), kidneys *(g)* are hydronephrotic with cortical and medullary cysts *(h)*. The use of 3D isotropic sampling makes it easy to extract corresponding sections from the two image volumes for comparison.

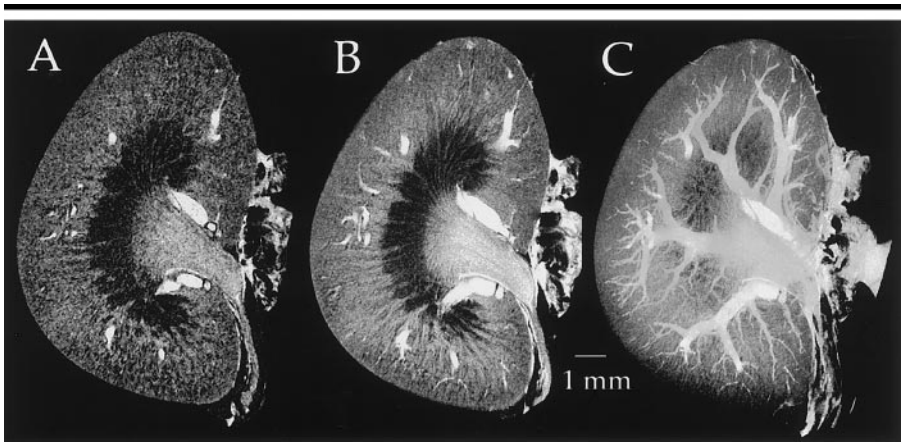

Figure 5. Images of the right kidney that has been removed from a perfusion-fixed mouse and imaged with a 256 × 512 × 512 array, resulting in 25-μm-thick voxels. In addition to the thinnest 25-μm-thick section of the kidney *(A)*, rendering techniques can produce a 250-μm-thick section *(B)*, and a 2,500-μm-thick slab *(C)*, in which nonvascular tissue is transparent. Because the specimen was not physically sectioned, 3D anatomic relationships such as the branching vasculature are undisturbed.

DISCUSSION

Increasing interest in molecular imaging has made it clear that radiologic imaging is

moving to a new phase in contributing to the understanding of human disease. There are several apparent areas for collaboration between molecular and cell biologists and our more traditional imaging community; for example, the development of new imaging probes. In this study, we posed another avenue of interdisciplinary growth, that is, the application of our imaging technologies to the immediate problems of linking genotype to phenotype in the exploding growth of mouse models. The methods we used are the first, to our knowledge, of a number that will translate the technologies of MR microscopy to those of MR histology. We believe this will become a routine tool for the analysis of the mouse morphologic phenotype.

The extension of MR imaging to MR microscopy has required far more than simply "turning up the resolution knob" on the imagers. In a similar fashion, the interpretation of MR histologic data will require more than a simple extension of conventional anatomic understanding to the mouse. The volume resolution in these studies of the mouse is more than 250,000-fold that of a typical image of the human body; therefore, it is not surprising that we are now looking at structures that have not been seen with conventional MR imaging. Certainly we see the mouse liver, but if one looks more closely at Figure 5, one can readily see the liver lobule. This intermediate structural detail between the organ and the cell is readily discerned on these images. A critical need in translating our technology to basic science will be the interpretation of images. Opportunities are abundant for the radiologist to collaborate with the pathologist and molecular biologist in what will surely be an exciting and challenging field—MR histology.

We articulated four ideas that collectively establish a new field of study. The four critical ideas are *(a)* the use of MR histology with very large 3D imaging arrays, *(b)* the use of active stains that are designed explicitly for MR histology, *(c)* the development of a standard protocol for morphologic phenotyping, and *(d)* the development of a Web-based archive for comparative phenotyping.

The technique is currently limited by long imaging time and lack of a common reference space. The use of multiple coils that allow simultaneous acquisition of data from several animals and the use of magnets with higher field strength will clearly improve efficiency. The development of common reference spaces and statistical atlases will be possible on the basis of the extensive work that has been done in the comparison of human brain studies (20).

As new stains are developed, new structures will become apparent. As new mouse models are developed, representative specimens from isogenic colonies will undergo perfusion fixation by using multiple active stains. They will be imaged according to the protocol described earlier. The whole mouse will be imaged at approximately 100-μm isotropic resolution; limited volumes of the intact specimen, at 50-μm isotropic resolution; and excised organs, at 25-μm isotropic resolution. The resulting data will be registered in a common space and stored in a Web-accessible archive.

These digital data are being assembled into a multidimensional atlas for publication on the World Wide Web, following a model of several current genome databases (21,22). As the Visible Human (23) has provided a common reference for human anatomy, we believe the much broader "Visible Mouse" atlas will provide a common morphologic reference for the anatomy of the normal mouse and a growing number of transgenic and knockout mice.

We believe that the methods described in this study and the resulting database under development will serve as the foundation for the new field of quantitative morphologic phenotyping in which MR histology is used.

Acknowledgments: The authors thank Drs Mike Hershfield and Susan Kelley of the Department of Medicine at the Duke University Medical Center for allowing us to image their uricase knockout mouse and for valuable discussions on the potential of morphologic phenotyping with MR microscopy. We are grateful to Dr Robert Maronpot at the National Institute of Environmental Health Sciences, Research Triangle Park, NC, for valuable discussions on the complementary nature of MR and conventional histology. We thank Boma Fubara for her technical assistance in performing the perfusions. We thank Elaine Fitzsimons for editorial assistance.

References

1. Abbott A. Database to standardize mouse phenotyping. Nature 1999; 401:833.
2. Cannon TD, van Erp TG, Huttunen M, et al. Regional gray matter, white matter, and cerebrospinal fluid distributions in schizophrenic patients, their siblings, and controls. Arch Gen Psychiatry 1998; 55: 1084–1091.
3. Filippi M, Iannucci G, Tortorella C, et al. Comparison of MS clinical phenotypes using conventional and magnetization transfer MRI. Neurology 1999; 52:588–594.
4. Lauronen L, Munroe PB, Jarvela I, et al. Delayed classic and protracted phenotypes of compound heterozygous juvenile neuronal ceroid lipofuscinosis. Neurology 1999; 52:360–365.
5. Franco F, Dubois SK, Peshock RM, Shohet RV. Magnetic resonance imaging accurately estimates LV mass in a transgenic mouse model of cardiac hypertrophy. Am J Physiol 1998; 274:H679–H683.
6. Jalanko A, Tenhunen K, McKinney CE, et al. Mice with an aspartylglucosaminuria mutation similar to humans replicate the pathophysiology in patients. Hum Mol Genet 1998; 7:265–272.
7. Kelly SJ, Delnomdedieu M, Oliverio MI, et al. Diabetes insipidus in uricase-deficient mice: a model for evaluating therapy with poly(ethylene glycol)-modified uricase. J Am Soc Nephrol 2001; 12:1001–1009.
8. Johnson GA, Thompson MB, Gewalt SL, Hayes CE. Nuclear magnetic resonance imaging at microscopic resolution. J Magn Reson 1986; 68:129–137.
9. Eccles CD, Callaghan PT. High resolution imaging: the NMR microscope. J Magn Reson 1986; 68:393–398.
10. Johnson GA, Hedlund LW, Cofer GP, Suddarth SA. Magnetic resonance microscopy in the life sciences. Rev Magn Reson Med 1992; 4:187–219.
11. Callaghan PT. Principles of nuclear magnetic resonance microscopy. Oxford, England: Oxford Science, 1993.
12. Hurlston SE, Cofer GP, Johnson GA. Optimized receiver coils for increased SNR in MR microscopy. Int J Imaging Syst Technol 1997; 8:277–284.
13. Lai CM, Lauterbur PC. True three-dimensional image reconstruction by nuclear magnetic resonance zeugmatography. Phys Med Biol 1981; 26:851–856.
14. Johnson G, Hutchison JMS, Redpath TW, Eastwood LM. Improvements in performance time for simultaneous three-dimensional NMR imaging. J Magn Reson 1983; 54:374–384.
15. Suddarth SA, Johnson GA. Three-dimensional MR microscopy with large arrays. Magn Reson Med 1991; 18:132–141.
16. Mendonca-Dias MH, Gaggelli E, Lauterbur PC. Paramagnetic contrast agents in nuclear magnetic resonance medical imaging. Semin Nucl Med 1983; 13:364–376.
17. Brasch RC. New directions in the development of MR imaging contrast media. Radiology 1992; 183:1–11.
18. Wehrli FW, MacFall JR, Glover GH, Grigsby N, Haughton V, Johansen J. The dependence of nuclear magnetic resonance (NMR) imaging contrast on intrinsic and pulse sequence timing parameters. Magn Reson Imaging 1984; 2:3–16.
19. Wehrli F, Shaw D, Kneeland J. Biomedical magnetic resonance imaging: principles, methodology, and applications. New York, NY: VCH, 1988.
20. Toga AW. Brain warping. San Diego, Calif: Academic Press, 1999.
21. The Jackson Laboratory. Mouse genome informatics: gene expression database. Available at: *www.informatics.jax.org/*. Accessed December 6, 1999.
22. The Jackson Laboratory. Mouse genome informatics: mouse genome database. Available at: *www.informatics.jax.org/*. Accessed December 6, 1999.
23. U.S. National Library of Medicine. The Visible Human Project. Available at: *www.nlm.nih.gov/research/visible/visible_human.html*. Accessed March 12, 2000.